Optical and Quantum Electronics manuscript No.
(will be inserted by the editor)

Analysis of the Photon-Photon Resonance Influence on the Direct Modulation Bandwidth of Dual-Longitudinal-Mode Distributed Feedback Lasers

Topi Uusitalo · Heikki Virtanen · Paolo Bardella · Mihail Dumitrescu

Received: date / Accepted: date

Abstract The paper explores the possibilities to extend the direct modulation bandwidth in dual-longitudinal-mode distributed feedback lasers by exploiting the photon-photon resonance induced by the interaction of the two modes in the laser cavity. The effects on the direct amplitude modulation and on the direct modulation of the difference frequency between the two modes are analyzed using simulation and experimental results. When the photon-photon resonance, which occurs at the difference frequency between the two modes, is properly placed at a higher frequency than the carrier-photon resonance, the small-signal amplitude modulation (AM) bandwidth of the laser can be significantly increased. However, both simulations and experiments point out that a high small-signal AM bandwidth does not lead to a high large-signal AM bandwidth if the small-signal modulation response has significant variations across the modulation bandwidth. The paper shows that a high large-signal AM bandwidth is obtained when the two modes are significantly unbalanced, whereas a high-bandwidth difference frequency modulation can be best detected when the two modes are balanced and the DC bias is properly chosen.

Keywords distributed feedback lasers · dual-mode lasers · surface gratings · nanoimprint lithography · photon-photon resonance · amplitude modulation · difference frequency modulation

1 Introduction

Despite the substantial efforts undertaken to increase the direct modulation bandwidth of lasers, no significant breakthrough has been made when the direct modulation bandwidth has been linked to the carrier-photon resonance (CPR) frequency, largely because the CPR has inherent physical limitations. A higher CPR

T. Uusitalo · H. Virtanen · M. Dumitrescu
ORC, Tampere University of Technology, P.O. Box 692, FIN-33101 Tampere, Finland
E-mail: topi.uusitalo@tut.fi

P. Bardella
Department of Electronics, Politecnico di Torino, Torino, Italy

frequency is obtained by reducing carrier and photon lifetimes but shortening these lifetimes too much ultimately prevents lasing.

However, since the direct modulation bandwidth can be extended considerably by introducing a supplementary high-frequency resonance of the laser, we have analyzed the effects of a high-frequency photon-photon resonance (PPR) on the laser modulation characteristics. The PPR has been obtained by the interaction of two longitudinal modes in dual-mode multi-section distributed feedback (DFB) lasers. The paper analyzes the dynamic behavior of the dual-longitudinal-mode DFB (DLM-DFB) lasers and the effects of mode interaction and photon-photon resonance strength and spectral position on the direct amplitude modulation and on the direct modulation of the difference frequency between the two modes.

The paper is structured as follows: In section 2 the theory behind PPR is introduced alongside descriptions of the simulation methods used. In section 3 both the simulation and measurement results are presented and discussed. Section 4 summarizes the most important findings and draws some conclusions.

2 Photon-Photon Resonance

Several different device variants have been investigated to exploit the PPR effect (Montrosset and Bardella, 2014). One example is a passive feedback DFB, which has extremely narrow operation domains where the dual-mode emission is stable enough to generate a PPR and the corresponding mode-beating signal (Radziunas et al, 2007). However, the authors show that by suppressing the CPR and PPR resonances the direct modulation bandwidth can be increased. Another method is to use a monolithic injection locking (Sung et al, 2003). The authors record a modulation bandwidth increase when the master and slave sections of the laser are locked to each other. Yet another method to generate dual-mode emission that has also been studied is a two-section DFB with independent drive currents and the same or slightly different Bragg frequencies in the two section (Wake, 1996). However, this type of laser has not been studied for PPR effects and increased modulation bandwidth.

Our method for generating the PPR is to use a multi-section monolithic DFB laser that exhibits dual-mode emission over a wide operation regime (Dumitrescu et al, 2016). The dual-mode emission is achieved by having $\pi/2$ phase-shifts periodically placed along the grating. When two or more periodically-placed phase-shifts are used, the grating reflectivity exhibits two maxima separated by approximately $2\times\lambda_{Bragg}/M$, where M is the number of grating periods between phase-shifts. When the two reflectivity maxima are placed at wavelengths around the peak gain wavelength the structure supports two modes placed next to the inner edges of the two reflectivity 'stopbands'. Therefore, the spectral spacing of the emitted modes can be roughly controlled by the number M of the grating periods between two phase-shifts and by the grating coupling coefficient and total grating length (which influence the width of the reflectivity 'stopbands'). Besides being structurally controlled, the mode spacing can be adjusted by the bias applied to the laser sections since carrier-density-induced refractive index changes shift the spectral positions of the reflectivity stopbands.

The exact dual-mode behavior also depends on several other factors besides the grating reflectivity, such as carrier and photon distributions and cavity dynamics,

which influence spatial (Otsuka et al, 1992) and spectral hole burning (Adams et al, 1983), and gain competition between the modes (Adams and Osihski, 1982; Lamb Jr, 1964).

2.1 Improved Rate Equation Model

When two (quasi-)phase-locked modes coexist in the laser cavity the optical confinement factor is dynamically dependent on the longitudinal position. A modified rate-equation model has been developed to take the PPR into account by treating the longitudinal confinement factor as a dynamic variable (Laakso and Dumitrescu, 2011):

$$\frac{d}{dt}\begin{bmatrix} dN \\ dN_p \end{bmatrix} = \begin{bmatrix} -\gamma_{NN} & -\gamma_{NP} \\ \gamma_{PN} & -\gamma_{PP} \end{bmatrix} \begin{bmatrix} dN \\ dN_p \end{bmatrix} + \begin{bmatrix} \frac{\eta_i}{qV} dI \\ (N_p v_g g + R'_{sp}) d\Gamma \end{bmatrix}, \tag{1}$$

where γ_{NN}, γ_{NP}, γ_{PN} and γ_{PP} are rate coefficients, as defined in (Coldren and Corzine, 1995). The modified rate equation model has a supplementary term $(N_p \times v_g \times g + R'_{sp})d\Gamma$, resulted from the (space and) time variation of the dual-mode confinement factor. The amplitude modulation transfer function, including the influence of the extra term, is:

$$H(\omega) = \frac{\eta_i}{qV} \frac{\int_0^T \frac{\gamma_{PN}}{\Delta} dt}{T} + \frac{1}{I_1 \cdot T} \cdot \int_0^T \frac{(\gamma_{NN} + j\omega) \cdot (N_p v_g g + R'_{sp})}{\Delta \cdot e^{j\omega t}} \cdot \frac{d\Gamma}{dt} dt, \tag{2}$$

where T is the time interval for which the phase difference between the two dominant longitudinal modes is maintained. The first term in Eq. (2) resembles the traditional modulation transfer function, with γ_{PN} and Δ taken as time-dependent, while the second term results from considering the (space and) time dependence of the confinement factor. This second term introduces the supplementary PPR peak placed at a frequency equal with the frequency difference between the two dominant longitudinal modes. The model indicates that a primary condition for achieving the PPR is to have the dominant modes phase-locked for long enough (i.e. quasi-phase-locked). Therefore, besides the large frequency difference between modes, the main reason for not achieving significant PPR peaks in the amplitude modulation response of conventional multimode lasers is that they do not provide a mechanism to maintain the phase difference between modes for long enough. It should however be noted that the difficulty in extending the direct laser modulation bandwidth by exploiting the PPR is not so much related to placing the PPR at high frequencies as it is related to achieving a flat modulation response between the CPR and the PPR.

2.2 Travelling-Wave Model

The dynamic behavior of the laser has been simulated with a finite-difference traveling-wave based method (Bardella and Montrosset, 2005). The total electric

field in the cavity is expressed as

$$E(z,t) = \left(E^{+}(z,t)\mathrm{e}^{-\mathrm{j}\pi z/\Lambda} + E^{-}(z,t)\mathrm{e}^{\mathrm{j}\pi z/\Lambda}\right)\mathrm{e}^{\mathrm{j}2\pi tc/\lambda_{\mathrm{B}}}, \tag{3}$$

where $E^{\pm}$ are the spatially-dependent slowly-varying forward and backward propagating field envelopes, normalized so that the photon density S is $|E^{+}|^2 + |E^{-}|^2$, Λ is the grating pitch and λ_B is the grating Bragg wavelength.

The equations for the propagating fields are coupled to the carrier rate equation, resulting a system of non linear differential equations, which are then discretized in time and space and integrated using the split-step algorithm (Kim et al, 2000):

$$\left(\frac{1}{v_g}\frac{\partial}{\partial t} \pm \frac{\partial}{\partial z}\right)E^{\pm}(z,t) = \delta E^{\pm}(z,t) + \mathrm{j}\kappa E^{\mp}(z,t) + S_{\mathrm{sp}}, \tag{4}$$

$$\frac{\partial}{\partial \mathrm{t}}N(z,t) = \frac{\eta_i I}{\mathrm{q}V} - \frac{N(z,t)}{\tau} - v_g\frac{\Gamma_{xy}g(z,t)}{1+\varepsilon S(z,t)}S(z,t), \tag{5}$$

with $\delta = \Gamma_{xy}g(z,t) - \alpha_l - \mathrm{j}\pi\left(\frac{2}{\lambda_B}n_{\mathrm{eff}}(z,t) - \frac{1}{\Lambda}\right)$, α_i material losses, κ grating coupling coefficient and S_{sp} spontaneous emission term. A linear dependence of the material gain g and of the refractive index n_{eff} on the carrier density is assumed.

This model is particularly suitable for the considered problem since the nonlinear interactions between the cavity modes (such as the ones generating the PPR) are automatically included in the calculation of $E^{\pm}$.

3 Results

Multi-section 1.3 and 1.55 µm DFB lasers with 3$^{\mathrm{rd}}$ order laterally-coupled ridge-waveguide (LC-RWG) surface gratings (Laakso et al, 2008) have been fabricated, without regrowth and using cost-effective UV nanoimprint lithography, from InP-substrate legacy epiwafers (with epilayer structures designed for Fabry-Pérot lasers). Two quasi-phase-locked longitudinal modes with frequency differences ranging from 14 GHz to 1.3 THz have been obtained by adjusting the longitudinal structures of the lasers (mainly by changing the number of periods between phase-shifts). Fig. 1a and 1b show measured and simulated dual-longitudinal-mode emission spectra with mode frequency differences of 47 GHz and 1 THz, respectively. The simulations were done with the commercial PICS3D package from Crosslight Software Inc. The red-shift of the measured spectra with respect to the simulations from Fig. 1 is due to a higher temperature in the measurements than in the simulations. This might be due to more heat generated by a lossy current injection and/or by inferior heat sinking in the measured devices.

3.1 Amplitude modulation

Because the amplitude modulation (AM) responses of the dual-mode lasers with big frequency differences between the two quasi-phase-locked modes are hampered

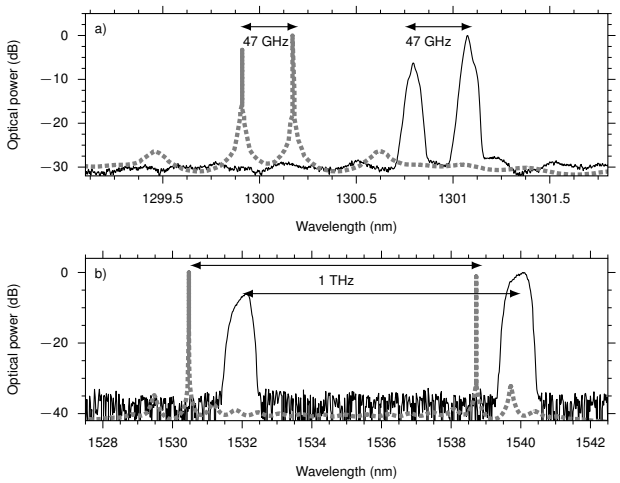

Fig. 1 Simulated (dotted line) and measured (solid line) dual-mode emission spectra with quasi-phase-locked longitudinal modes having a) 47 GHz and b) 1.0 THz frequency spacing

by the large and deep dips between the CPR and the PPR, we have targeted mainly PPR frequencies below and around 20 GHz.

In order to evaluate the effects of PPR on the laser AM, two types of DFB lasers have been fabricated from the same legacy epiwafer (with the epilayer structure intended for the fabrication of Fabry-Pérot lasers at 1.55 µm) and in the same fabrication run (with similar LC-RWG grating structures). The difference between the two types of DFB lasers was only related to their longitudinal structures: one type had a single $\lambda/4$ phase-shift in the middle of the cavity and a single longitudinal mode emission, whereas the second type had two $\lambda/4$ phase-shifts placed in order to obtain quasi-phase-locked dual-longitudinal-mode emission and a corresponding PPR at 14 GHz.

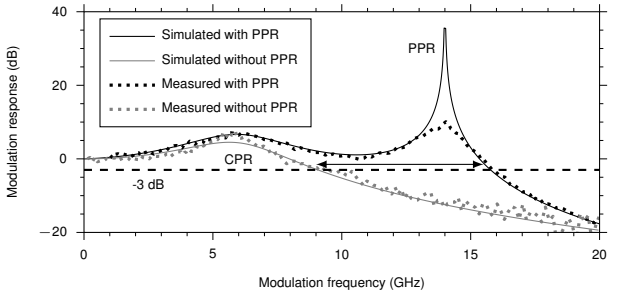

Fig. 2 Measured and simulated small-signal AM responses for two types of DFB lasers fabricated from the same epiwafer in the same fabrication run but with different longitudinal structures. The DFB laser with one $\lambda/4$ phase-shift emits a single-longitudinal mode, whereas the DFB laser with two $\lambda/4$ phase-shifts emits two quasi-phase-locked modes and exhibits a PPR peak at 14 GHz in the small-signal AM response. The attained small-signal AM bandwidth increase, shown with the arrow, is more than 5 GHz

Fig. 2 shows measured and simulated direct AM responses for both types of lasers, with and without PPR, illustrating the increase in small-signal AM bandwidth obtained by exploiting the PPR. The AM simulation for the laser with PPR was fitted to the measurement by assuming a side-mode-suppression-ratio (SMSR) of 23 dB between the two quasi-phase-locked modes. The sharper PPR peak in the simulation is due to the fact that noise and averaging are left out in the model.

Taking into account that the flatness of the small-signal AM response is important in extending the small-signal AM bandwidth, we have studied the possibility to adjust the PPR position and the flatness of the AM response between the CPR and PPR by adjusting the bias currents of the laser sections. Fig. 3a illustrates the measured changes in the PPR and CPR frequencies with changing the bias in one sections of a 1.6 mm long multi-section dual-longitudinal-mode DFB (DLM-DFB) laser emitting at 1.55 µm. Because throughout the whole bias variation range the two longitudinal modes are in relatively good balance, the PPR peak dominates CPR and a flat AM response cannot be achieved. Fig. 3b shows the measured tuning of the PPR frequency and the CPR changes induced by adjusting one of the bias currents for a 1.5 mm long multi-section DLM-DFB laser emitting at 1.3 µm. Here the CPR-PPR gap is filled when the PPR is brought closer to the CPR. Also the AM response is flatter between the CPR and PPR because the balance between the two longitudinal modes is reduced. The CPR peak changes in Fig. 3a and Fig. 3b because the carrier and photon distributions within the cavity also undergo changes when one of the laser bias currents is adjusted.

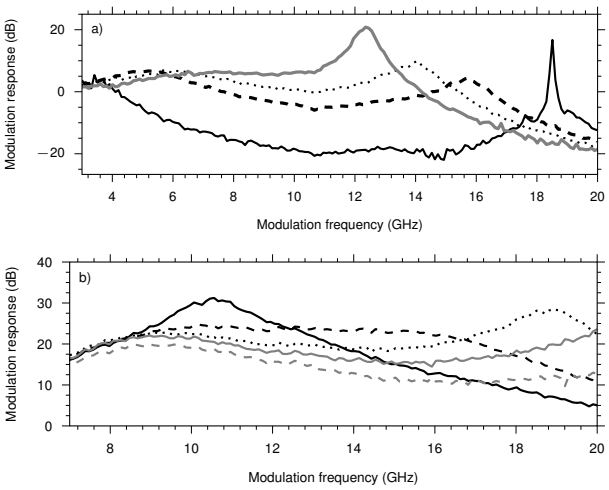

Fig. 3 Measured small-signal AM response for a) 1.6 mm long multi-section DLM-DFB laser emitting at 1.55 µm and for b) 1.5 mm long multi-section DLM-DFB laser emitting at 1.3 µm. The current of the section farthest from the lasing facet is increased for modulation responses progressing from black solid lines to dashed lines to dotted lines and to gray solid lines

Since the −3 dB small-signal AM bandwidth may not be indicative of the large-signal modulation capability, particularly in case of a small-signal AM response with substantial variations across the bandwidth, we have also analyzed the small-signal AM response and the corresponding large-signal modulation capability us-

ing a Finite-Difference Travelling-Wave program (Bardella and Montrosset, 2012). Fig. 4a shows the small-signal AM response simulated for three different phases of the cleaved-facet reflection in a multi-section DLM-DFB laser. A similar effect can be obtained by changing the bias current in the DLM-DFB laser section farthest from the lasing facet, like in the experiments illustrated in Fig. 3.

Large-signal eye diagrams were calculated for the three small-signal AM cases of Fig. 4a, using a non-return-to-zero pseudorandom bit sequence signal at different modulation bit rates. The cases were chosen to compare the situation when the PPR peak is small, under the −3 dB level and with minimal influence on the small-signal AM bandwidth (case 1, solid line in Fig. 4a); the situation when the PPR peak is moderate and the AM response is extended in a relatively flat way (case 2, dashed line in Fig. 4a); and the situation when the PPR peak is very pronounced (case 3, dotted line in Fig. 4a).

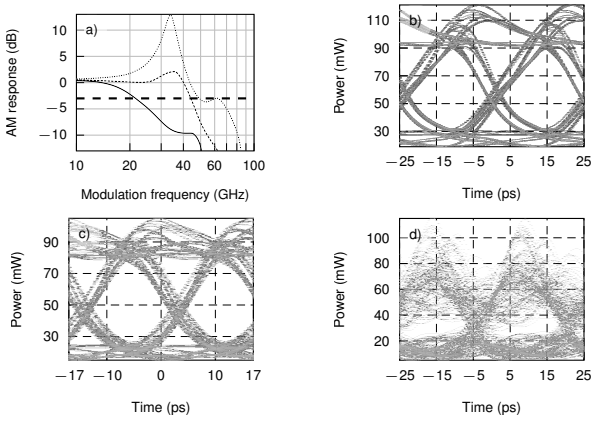

Fig. 4 a) Simulated small-signal AM response for different phases of the cleaved facet reflection in a multi-section DLM-DFB laser with high-frequency PPR. Case 1: solid line, cleaved facet reflection phase $\phi_A = 40°$. Case 2: dashed line, $\phi_A = 80°$. Case 3: dotted line, $\phi_A = 140°$. b) 40 Gbit/s eye diagram simulated for case 1, with an extinction ratio (ER) = 6 dB. c) 60 Gbit/s eye diagram simulated for case 2, with ER = 4.5 dB. d) 40 Gbit/s eye diagram simulated for case 3

An eye diagram with a reasonably good extinction ratio (ER = 4.5 dB) could be obtained, beyond the −3dB small-signal AM bandwidth, at 60 Gbit/s for case 2. The simulation for case 3 shows that a strong PPR peak is dramatically reducing the eye opening at 40 Gbit/s, although a good large-signal AM response should be achieved at this rate for a flat small-signal AM response. This result gives the indication that a strong presence of the second mode (i.e a good balance between the two dominant longitudinal modes and a strong PPR) does not bring an increase in the large-signal AM bandwidth.

Interestingly, a good 40 Gbit/s large-signal AM response, beyond the −3dB small-signal AM bandwidth, could be obtained in the case 1, when the PPR peak is well below the −3 dB level and does not influence significantly the small-signal AM bandwidth. This result is consistent with the rate-equation simulations illus-

trated in Fig. 2, indicating that the two dominant longitudinal modes should be significantly unbalanced in order to increase the AM bandwidth.

3.2 Difference frequency modulation

Albeit it hampers the extension of the AM bandwidth, a well balanced dual-longitudinal-mode emission could be exploited in frequency-modulated (FM) data transmission schemes by imprinting the signal in the difference frequency between the two dominant longitudinal modes. The tunability of the difference frequency is a prerequisite for difference frequency modulation (DFM). As indicated by the bias-induced frequency shifts of the PPR shown in Fig. 3, the inter-mode difference frequency of the DLM-DFB lasers is tunable over a wide range simply by tuning the bias currents of the laser sections.

Some measurements illustrating the inter-mode difference frequency change with the bias applied to one of the DLM-DFB laser sections are presented in Fig. 5. Only after a large increase in the injected current density the side modes become comparable with the two dominant longitudinal modes (as shown in Fig. 5a) but even then the difference frequency signal can be detected due to the quasi-phase-locking of the two longitudinal modes promoted by the grating structure.

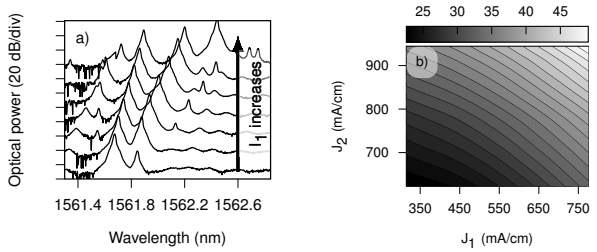

Fig. 5 a) Dual-longitudinal-mode spectrum variation when the current density J_1 is increased by 653 mA/cm^2 in the DLM-DFB laser section next to the output facet. b) Difference frequency variation (in GHz) between the two dominant longitudinal modes, measured with an ESA from the photodetected mode-beating signal, as a function of the current densities in the first two DLM-DFB laser sections

The bias map given in Fig. 5b shows that the change in the difference frequency is smooth and continuous with changing the bias currents in two different sections of the DLM-DFB laser. The stationary difference frequencies in the bias map have been obtained from the photodetected mode-beating signal recorded with an electric spectrum analyzer (ESA). This was done since the frequency resolution achieved with the ESA is at Hertz-level, whereas the available optical spectrum analyzer (OSA) provided only 2 GHz frequency resolution.

The dynamic behavior of the multi-section DLM-DFB lasers was studied in order to evaluate the possibility to exploit the difference frequency modulation in high-speed applications. In a first instance the bias of the first section of the DLM-DFB lasers was modulated with a sinusoidal signal of varying frequencies. The laser output was photodetected with a high bandwidth photodiode (PD)

and the photodetected signal was amplified and down-shifted in frequency by mixing it with the signal from a microwave local oscillator (LO) in order to enable the measurement of the generated signal with a high bandwidth oscilloscope. A windowed fast Fourier transform (FFT) with a Gaussian window function (i.e. a Gabor transform) was applied to the time-domain difference frequency signal collected by the oscilloscope.

Fig. 6 shows spectrograms obtained by displaying the time-sequence of the window Fourier transforms for four different sinusoidal laser-bias modulation frequencies f_{mod} : 10 MHz, 100 MHz, 500 MHz and 1 GHz. The beat signal spectrum variation according to the difference frequency change induced by the sinusoidal modulating signal is clearly visible. Due to the limited oscilloscope bandwidth and sampling frequency (20 GHz, 50 GS/s), the frequency resolution of the spectrograms suffers when the modulation frequency increases since fewer spectral samples can be collected when more time-domain signal variations are recorded per unit time.

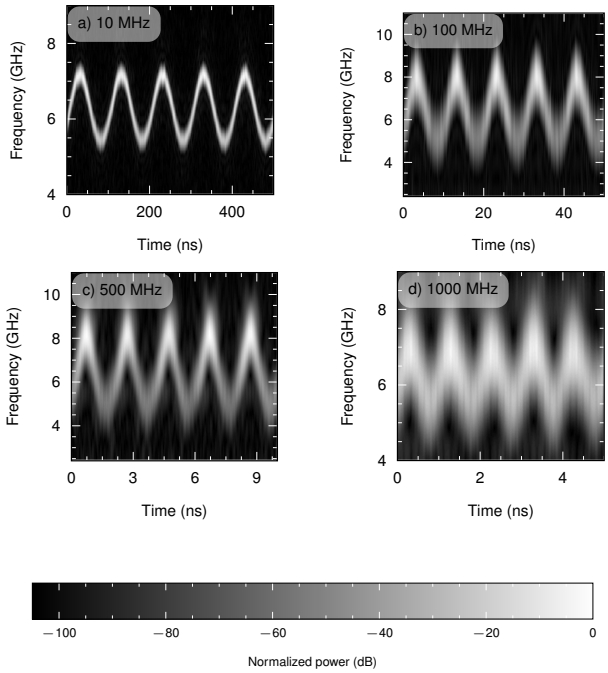

Fig. 6 Spectrograms showing the Gabor transforms of the mode-beat signals obtained from photodetecting the output of the directly modulated DLM-DFB laser. The frequency resolution suffers at higher modulation frequencies because there are less samples in the Fourier transform window due to the limited sampling rate of the oscilloscope

The sidebands of the frequency-modulated mode-beating signal spectra shown in Fig. 7 prove that the inter-mode difference frequency can be modulated by sinusoidal signals with frequencies up to 3 GHz. The modulation signal delivery to the DLM-DFB laser is critical at higher frequencies since impedance matching becomes important and the modulation signal strength has to be increased if an

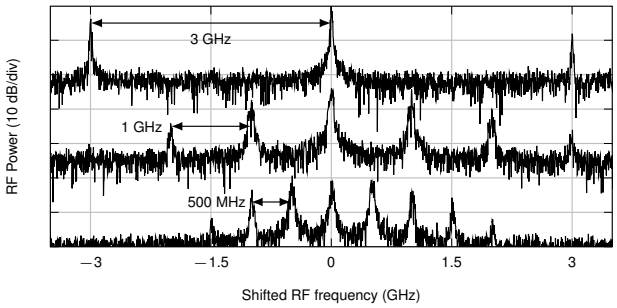

Fig. 7 Spectra of the photodetected mode-beat signal when the bias of one of the DLM-DFB laser sections is sinusoidally modulated at 500 MHz, 1 GHz and 3 GHz. The distance between the FM side bands and the carrier is the same as the sinusoidal modulation frequency

impedance-matched delivery circuit is not employed. In the DFM spectra presented in Fig. 7 the modulation signal is increased by 7 dB when the sinusoidal modulation frequency increases from 500 MHz to 1 GHz, and by another 12 dB when the sinusoidal modulation frequency is increased again from 1 GHz to 3 GHz. In fact we have detected sidebands in the DFM spectra up to 10 GHz sinusoidal modulation frequencies but they were close to the noise floor due to the poor delivery of the modulation signal to the laser.

Unfortunately, detecting the instantaneous difference frequency change induced by large-signal modulation is difficult. In order to prove that the large-signal difference-frequency modulation can be recovered from the photodetected mode-beating signal we have performed the signal recovery in post-processing. The post-processing procedure is summarized in Fig. 8. First, the photodetected mode-

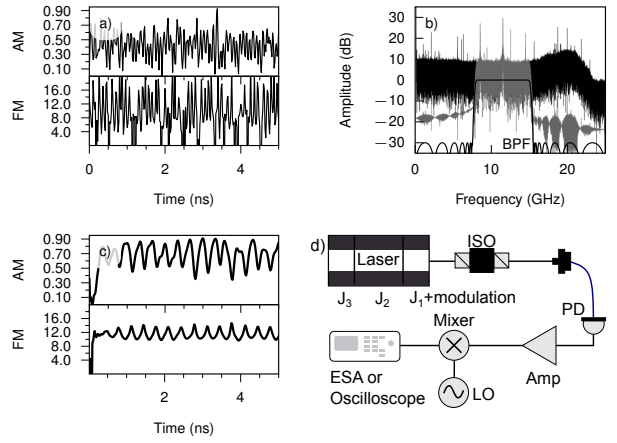

Fig. 8 Illustration of the post-processing procedure for difference frequency demodulation: a) Hilbert transforms of the signal recorded after photodetection and mixing, showing the envelope (AM) and the instantaneous frequency (FM); b) FFT of the signal with and without IIR filtering; c) Hilbert transform of the IIR filtered signal; d) The measurement setup employed for collecting the signals for post-processing (ISO: Optical isolator, PD: Photodiode, Amp: RF amplifier, LO: Local Oscillator)

beating signal is frequency down-shifted by mixing with a local oscillator and the resulted FM signal is recorded with a high-speed oscilloscope (shown in Fig. 8a after the application of a Hilbert transform). Then the recorded time-domain signal is transferred to the frequency domain with FFT, and the center frequency of the resulting FM comb is saved. In order to reduce the noise in the signal, a band pass Chebyshev type II infinite impulse response (IIR) filter was used (because it has a relatively good slope at the pass band edges and it doesn't have ripples in the pass band) (Fig. 8b). The filtered time-domain signal is then Hilbert transformed in order to get the amplitude variation of the difference frequency signal as well as its instantaneous frequency (Boashash, 1992) (Fig. 8c).

The signals extracted by post-processing can be used to generate eye diagrams, like the ones presented in Fig. 9. It should be noted that, due to the frequency down-shifting by mixing with the local oscillator, the extracted difference frequency is flipped in frequency (i.e. large difference frequencies are extracted as small mode-beat signal frequencies and vice-versa).

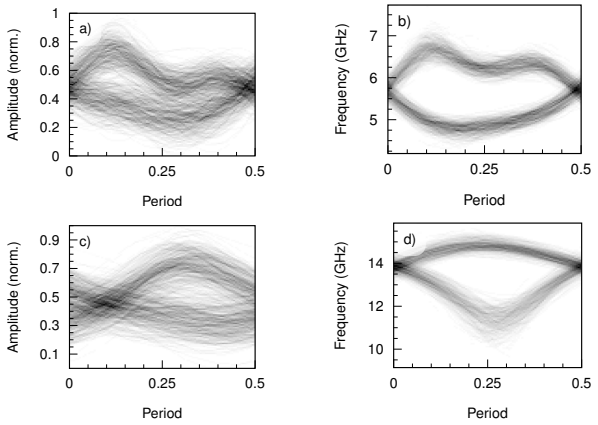

Fig. 9 Eye diagrams of the post-process-extracted difference frequency signal resulted from directly modulating the first section of the laser with a 1 GHz (a-b) and with a 3 GHz (c-d) signal. a) and c) give the extracted amplitude modulation, whereas b) and d) give the difference frequency modulation

The comparison of the extracted AM and FM eye diagrams indicate that a parasitic AM accompanies the DFM, somehow similarly as a parasitic FM (i.e. chirp) accompanies the amplitude modulation of single-mode lasers.

The large-signal modulation results have been simulated in steady-state frequency domain with a transfer matrix method (TMM) program. In this approach the effect of the bias modulation has been modeled as carrier-density-induced refractive index changes. The transfer matrix model only considers the steady-state optical properties of the laser, and other effects, particularly dynamic effects, are omitted. The TMM-calculated bias-induced steady-state difference frequency changes corresponding to the post-process-extracted 1 GHz eye diagrams are given in Fig. 10. The difference frequencies obtained by the post-processing of the measured signal and the TMM-simulated difference frequencies differ in their absolute

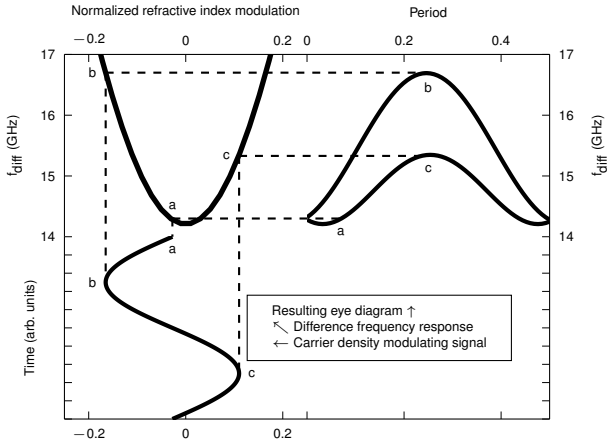

Fig. 10 TMM simulation of the 1 GHz difference frequency eye diagram of Fig. 9b obtained by post-processing

values for multiple reasons: because the measured values have been down-shifted in frequency, because the coupling coefficients might be different between simulation and measurement, and because the simulation doesn't take into account electrical and dynamic effects.

Despite its limited accuracy, the TMM results indicate that the main cause for the 1 GHz eye diagram asymmetry is the DC point where the bias modulation is applied. The TMM simulations of the large-signal modulation at 3 GHz (shown in Fig. 11) indicate that the superior eye diagram symmetry and the large eye diagram opening resulted from post-processing and shown in Fig. 9d are mainly induced by a better DC bias point.

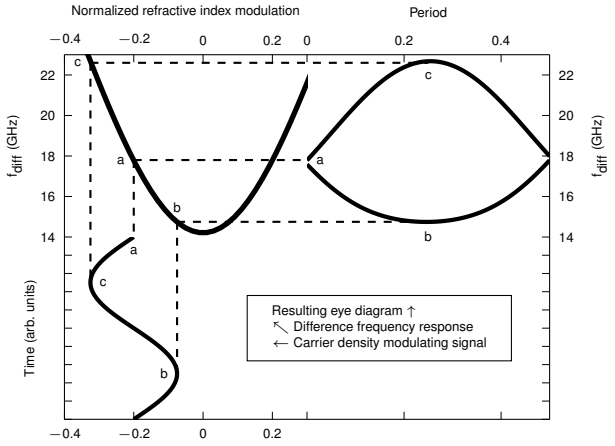

Fig. 11 TMM simulation of the 3 GHz difference frequency eye diagram of Fig. 9d obtained by post-processing

4 Conclusions

The presented simulation and experimental results show that quasi-phase-locked dual-longitudinal-mode emission and the associated photon-photon resonance can be exploited for increasing the direct amplitude modulation (AM) bandwidth beyond the limitations set by the carrier-photon resonance. The extension of the AM bandwidth is obtained when the photon-photon resonance frequency is placed relatively close to the carrier-photon resonance frequency and one of the two grating-favored longitudinal modes is significantly weaker than the other one.

The presented simulation and experimental results also show that direct modulation of the difference frequency between the dominant modes of dual-longitudinal-mode (DLM) DFB lasers can be exploited for high-bandwidth frequency-modulation (FM) data transfer. The difference frequency modulation (DFM) analysis leads to several conclusions: i) significant continuous difference frequency changes can be obtained by changing the bias in one of the DLM-DFB laser sections; ii) a good dual-longitudinal-mode balance favors difference frequency detection; iii) the difference frequency can be modulated with very high rates; iv) the DC bias point at which the modulation is applied has a significant influence on the possibility to transmit and extract accurately the signal imprinted in the difference frequency. Overall, the dual-longitudinal-mode difference frequency experiments and simulations indicate that the DFM can be effectively employed in high-bandwidth FM optical transmission if practical real-time demodulation schemes are developed.

References

Adams M, Osihski M (1982) Longitudinal mode competition in semiconductor lasers: Rate equations revisited. IEE Proceedings I-Solid-State and Electron Devices 129(6):271–274

Adams M, et al (1983) Influence of spectral hole-burning on quaternary laser transients. Electronics Letters 16(19):627–628

Bardella P, Montrosset I (2005) Analysis of self-pulsating three-section dbr lasers. IEEE Journal of Selected Topics in Quantum Electronics 11(2):361–366, DOI 10.1109/JSTQE.2005.845608

Bardella P, Montrosset I (2012) Design and simulation of dbr lasers with extended modulation bandwidth exploiting photon-photon resonance effect. In: European Conference on Integrated Optics, ECIO'2012, Sitges (Spain), April 18-20, 2012.

Boashash B (1992) Estimating and interpreting the instantaneous frequency of a signal. i. fundamentals. Proceedings of the IEEE 80(4):520–538

Coldren L, Corzine S (1995) Diode lasers and photonic integrated circuits. Wiley&Sons, NY

Dumitrescu M, Uusitalo T, Virtanen H (2016) Laser structure. Patent Cooperation Treaty application PCT/EP2016/064476

Kim B, Chung Y, Lee J (2000) An efficient split-step time-domain dynamic modeling of dfb/dbr laser diodes. IEEE Journal of Quantum Electronics 36(7):787–794, DOI 10.1109/3.848349

Laakso A, Dumitrescu M (2011) Modified rate equation model including the photon–photon resonance. Optical and quantum electronics 42(11-13):785–791

Laakso A, Dumitrescu M, Viheriälä J, Karinen J, Suominen M, Pessa M (2008) Optical modeling of laterally-corrugated ridge-waveguide gratings. Optical and quantum electronics 40(11-12):907–920

Lamb Jr WE (1964) Theory of an optical maser. Physical Review 134(6A):A1429

Montrosset I, Bardella P (2014) Laser dynamics providing enhanced-modulation bandwidth. In: Proceedings of SPIE - The International Society for Optical Engineering, vol 9134

Otsuka K, Georgiou M, Mandel P (1992) Intensity fluctuations in multimode lasers with spatial hole burning. Jpn J Appl Phys 31(9A Pt 2)

Radziunas M, Glitzky A, Bandelow U, Wolfrum M, Troppenz U, Kreissl J, Rehbein W (2007) Improving the modulation bandwidth in semiconductor lasers by passive feedback. IEEE Journal of selected topics in Quantum Electronics 13(1):136

Sung HK, Jung T, Wu MC, Tishinin D, Tanbun-Ek T, Liou K, Tsang W (2003) Modulation bandwidth enhancement and nonlinear distortion suppression in directly modulated monolithic injection-locked dfb lasers. In: Microwave Photonics, 2003. MWP 2003 Proceedings. International Topical Meeting on, IEEE, pp 27–30

Wake D (1996) Optical devices for millimetre-wave transmission. In: Microwave Photonics, 1996. MWP '96. Technical Digest., 1996 Internatonal Topical Meeting on, pp 145–148, DOI 10.1109/MWP.1996.662091